

# PARAMETER ESTIMATION AND TREATMENT OPTIMIZATION IN A STOCHASTIC MODEL FOR IMMUNOTHERAPY OF CANCER

MODIBO DIABATE, LOREN COQUILLE, AND ADELIN SAMSON

**Abstract.** We study the stochastic model developed by Baar et al., 2015 for the modeling of immunotherapy against melanoma skin cancer. In the first part, we estimate the parameters of the deterministic limit of the model based on the biological data of tumor growth in mice which are provided in Landsberg et al., 2012. The main statistical tools we use are the NonLinear Mixed Effects Models (NLMEM) and the Stochastic Approximation Expectation Maximization (SAEM) algorithm. With the estimated parameters, we head back to the stochastic model and calculate the probability that the T cells all get exhausted during the treatment. We show that for biologically reasonable values of the parameters, an early relapse is due to stochastic fluctuations (complete T cells exhaustion) with a non negligible probability. In the second part, assuming that the relapse is related to the T cell exhaustion, we propose to optimize the treatment plan (treatment doses and restimulation times) by minimizing the T cell exhaustion probability at different stages of the disease evolution.

## 1. INTRODUCTION

Cancer is a group of more than 100 different diseases causing a large number of deaths a year worldwide [15]. It begins when cells start to grow uncontrollably due to genetic changes which impair their normal evolution. It can develop almost anywhere in the body. Cancer is a complex disease, difficult to study biologically (expensive and time consuming to experiment with animals and humans). In this context, mathematical modeling can be an excellent tool for emitting or confirming biological assumptions with less expensive experiments.

When it is diagnosed quickly, cancer can be treated by chemotherapy, surgery, radiotherapy or by immunotherapy [1, 16, 23, 31]. Immunotherapy is a recent treatment that reactivates the immune system to kill cancer cells. In this paper we are interested by the Adoptive Cell Transfer (ACT) therapy to treat melanoma in mice with cytotoxic T cells, as experimented by Landsberg et al., 2012. This immunotherapeutic approach involves the stimulation of T cells which recognize one specific type of melanoma tumor cells (differentiated melanoma cells) through special markers on their surface. The stimulated T

---

*Key words and phrases.* Immunotherapy, T cell exhaustion, Stochastic modeling, Mixed Effects Models, Treatment Optimization.

This work has been partially supported by the LabEx PERSYVAL-Lab (ANR-11-61 LABX-0025-01). The authors would like to warmly thank Meri Rogava, Thomas Tüting and Michael Hölzel for fruitful discussions and for providing important medical informations, Jennifer Landsberg for providing the database used in this paper, and the Data Institute Univ. Grenoble Alpes for allowing computing time on the cluster "Luke" .

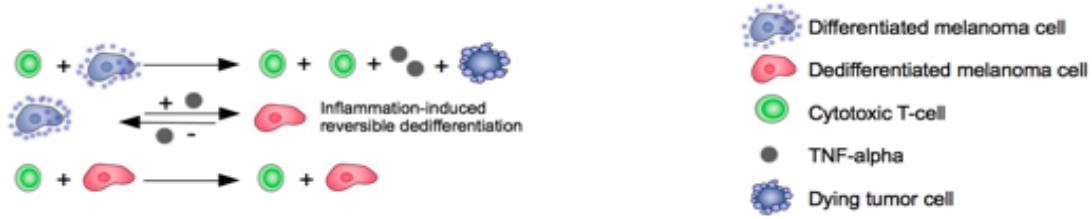


FIGURE 1. Main cell interactions in ACT Therapy: The killing of a differentiated melanoma cell by a T cell produces more T cells and cytokines  $TNF_\alpha$  (first line); the switch between differentiated and dedifferentiated melanoma cells is reversible (second line); a T cell cannot kill a dedifferentiated melanoma cell (third line) [4, 22].

cells are then able to kill these differentiated melanoma cells. The authors of [22] showed that during the inflammation induced by the therapy, pro-inflammatory cytokines called  $TNF_\alpha$  (Tumor Necrosis Factor) which are released in the body enhance a cell-type switch: the markers on the differentiated cancer cells disappear. They become dedifferentiated, and cannot get killed by T cells anymore. The resulting tumor tissue consists of both differentiated and dedifferentiated melanoma cells. Note that the switch is reversible (i.e, the melanoma cells can recover their initial type) and it does not require cell division or mutation.

Figure 1 illustrates the described interactions between cells during the treatment: the production of more T cells (plus the production of cytokines  $TNF_\alpha$ ) when a T cell kills a differentiated melanoma cell; the cell-type switch between differentiated and dedifferentiated melanoma cells; and the fact that a T cell cannot kill a dedifferentiated melanoma cell.

In immunotherapy (as in other treatments against cancer) the relapse is one of the main problems to manage. The authors of [4, 22] describe two kinds of relapse in the ACT therapy. First, T cells only recognize the differentiated cancer cells through special markers and not the dedifferentiated cancer cells that do not possess these markers on their surface. Thus, T cells are not capable of killing these dedifferentiated cells, which growth implies a relapse as shown on Figure 2. Second, T cells can become exhausted (their quantity falls down below a certain threshold) and they no longer kill differentiated cancer cells thus causing a relapse. This problem was addressed in [22] by T cells restimulation, which only lead to a delay in the occurrence of the relapse.

In these recent years, a lot of potentials have been seen in immunotherapy treatments, including the possibility of higher effectiveness [32] with lower side effects. It should be noted that, while immunotherapy techniques have shown very few and less serious side effects, long-term effects have not yet been studied in clinical trials. These promising new treatments are thus still to be understood. An alternative to long clinical trials which are costly is to study long term effects (treatment failure and relapse) through the development of mathematical models. Numerous mathematical models have been proposed for the cancer study: deterministic models mainly based on partial differential equations or ordinary differential equations [5, 26, 35, 36], stochastic models like individual-based

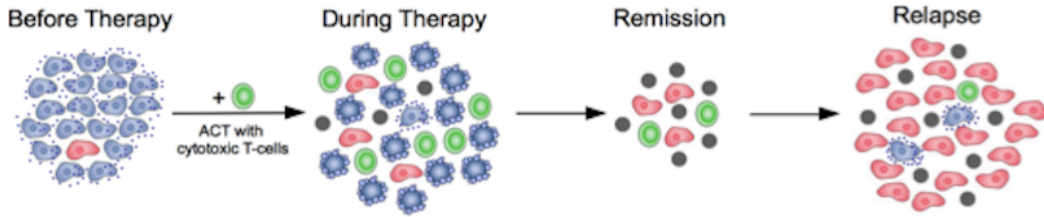


FIGURE 2. Relapse with dedifferentiated melanoma cells (in red) not killed by T cells [22]. The ACT therapy induces an inflammation and the melanoma cells react to this environmental change by switching their type (special markers on the differentiated melanoma cell surface disappear). The T cells are not capable of killing switched differentiated melanoma cells, and a relapse is observed: the tumor grows again. The switch thus allows tumors to be resistant to the therapy.

models or diffusion models [4, 9, 27] and often a combination of both [2, 29]. Longitudinal data are very common in cancer studies. Mixed effects models [28] are well adapted to such data and are often involved in parameter estimation in cancer models [7, 13, 17]. Maximum likelihood methods are used in [3] for estimating the growth function of tumors and in [20] to estimate the growth and metastatic rates of primary breast cancer; bayesian methods like Approximate Bayesian Computation (ABC) are used in [34] for analyzing colorectal cancer or in [37] for investigating on breast cancer dormancy.

The purpose of the present paper is to study the relapse and failure of skin cancer immunotherapy in mice using mathematical models. First, we estimate the parameters of the mathematical model developed by Baal et al. [4] which is adapted to the problem. Then, with the estimated parameters, we study the treatment relapse and failure focusing on T cell exhaustion and propose to optimize the treatment plan. The stochastic individual-based model recently proposed by [4] aims to model the ACT therapy in [22]. Its main features are: modeling the reproduction and the death of cancer cells and active T cells with birth and death processes [19] (the stimulation of T cells is modeled as birth of active T cells and their exhaustion as death of active T cells); modeling the switch between the two types of melanoma cancer cells; taking into account the interactions between cancer cells and T cells in a predator-prey framework [6, 11]. The different events (reproduction, death and switch events) occur at exponential random times in the model calibrated by rate parameters. The limit in large population (large number of cells) of the stochastic model is expressed in the form of a deterministic differential system [4]. The authors of [4] have provided a set of biologically reasonable parameters for which the stochastic system exhibits exhaustion of the T cells with high probability. However, these parameters have been calibrated numerically [4] but not estimated from real data. Our first objective is thus to estimate these parameters from real biological data. The direct estimation of parameters in the stochastic model is problematic due to its likelihood function defined as a multiple integral over a high dimension event space. To the best of our knowledge, there exists no statistical method to estimate the parameters of such models. As an approximation, we consider the likelihood of the limiting deterministic differential system.

We therefore estimate the parameters of the model through its deterministic limit using experimental data of tumor growth in mice provided by [22]. The database is composed of tumor size measurements along time in three groups of mice: a control group showing the tumor growth in absence of treatment, a group treated with ACT therapy and a group with ACT therapy and restimulation, i.e. reinjection of T cells. This last group allows to study the effect of the restimulation on the relapse. We analyze these longitudinal data simultaneously with a Non-Linear Mixed Effects Model (NLMEM) that takes into account the variability between the mice (population and individual parameters are estimated) [28]. The Stochastic Approximation Expectation Maximization (SAEM) algorithm [12] is used to estimate the parameters of the NLMEM.

Once the parameters have been estimated, the T cell exhaustion phenomenon is studied by heading back to the stochastic model. Indeed, complete exhaustion is a purely stochastic phenomenon which is not modeled by the deterministic system. As T cell exhaustion can be a rare event, we estimate it using a splitting Monte Carlo method adapted to rare event probability estimation [18, 25]. We observe that, in the range of parameters estimated from real data, the exhaustion probability can be large, which confirms a conjecture in [4].

As this kind of relapse can be delayed by restimulation of T cells, our second objective is to optimize the ACT protocol in this sense. We propose a treatment optimization plan based on the computation of optimal treatment doses and restimulation times by minimizing the T cell exhaustion probability at different stages of the disease evolution.

The paper is organized as follows. In Section 2 we present the experimental data used for parameter estimation. In Section 3, the stochastic model and its deterministic limit are described. In Section 4, we first present the statistical tools involved in the parameter estimation of the deterministic system, as well as the estimated parameter values. Second, we describe the T cell exhaustion probability estimation procedure and estimate the exhaustion probability as a function of the T cells death rate. In Section 5, we perform the ACT treatment optimization and present the related results.

## 2. EXPERIMENTAL DATA

We first describe the experimental setup of [22], from which we use the data. Initially a small number of melanoma cells is placed inside each mouse of the experiment. So, the initial size of the tumor is very small. Mice are then split into 3 groups: untreated mice playing the role of a control group (denoted CTRL) and treated mice composed of two subgroups: mice treated once with ACT therapy (denoted ACT) and mice treated twice with ACT therapy (denoted ACT+Re). After 70 days (at time  $t_a = 70$ ), mice of the groups ACT and ACT+Re receive a dose  $d_{70}$  of a T cell stimulant activating 2000 T cells and conferring them the ability to kill differentiated melanoma cells. The mice in the group ACT+Re receive an additional dose  $d_{Re}$  of the T-cell stimulant after 160 days re-activating 2000 T cells .

During the experiment, the tumor development is measured by palpation when the tumor is small and digital photography when the tumor is larger. The tumor size is measured weekly using a vernier caliper and recorded as mean diameter [22]. The database contains longitudinal data for 19 mice (after eliminating the mouse number 16 which has only two

observations). It is composed of 5 mice of the group CTRL (with an average number of 10 observations); 7 mice of the group ACT (with an average number of 26 observations); and 7 mice of the group ACT+Re (with an average number of 33 observations).

The measure of tumor size less than 2 mm is very inaccurate due to the difficulties of palpation. Thus, these values are left censored (they represent numbers in the range  $]0, 1.99[$ ). For tumor size between 2 mm and 3 mm, the inaccuracy is still important on the measures, about 1 mm. These values are interval censored between  $[2, 3]$ . Mice with tumor size exceeding 10 mm or showing signs of illness are killed. This means that for some mice, the last measurement indicating 10 mm is considered to be 10 mm or more, and are considered as right censored (they represent numbers in the range  $[10, +\infty[$ ). The other tumor sizes between 3 mm and 10 mm are considered correctly measured with a measurement accuracy around 0.5 mm.

Figure 3 represents the evolution of the tumor diameter along time for all the mice in the database. The three censorships are illustrated by aligned horizontal points. Excluded the observations at  $t_0 = 0$ , all the observations of the mice in the group CTRL are greater than 2 mm, so they are not concerned by the left-censorship. Observe that the three groups of mice are distinguished on the figure by the rapidity in the evolution of their tumor size: the CTRL mice (in blue) correspond to the mice whose tumor size reaches quickly 10 mm around the 100th day, the ACT mice (in red) correspond to the mice whose tumor size reaches 10 mm between the 240 and 300 days and finally the ACT+Re mice (in green) correspond to the mice whose tumor size reaches 10 mm beyond the 300th day. The treatment and retreatment times are indicated by (black) vertical dotted lines. We distinguish two phases in the ACT therapy (for treated mice): the growth phase (before  $t_a = 70$ ) and the treatment phase (after  $t_a = 70$ ). Note that the mice in the group CTRL have only the tumor growth phase.

### 3. MODELING TUMOR GROWTH UNDER TREATMENT

**3.1. Stochastic model.** The stochastic model proposed in [4] for tumor growth under ACT therapy consists in a four-dimensional continuous time Markov process  $Z(t) = (M(t), D(t), T(t), A(t)) \in \mathbb{N}^4$  with  $M(t)$  the population of differentiated melanoma cells,  $D(t)$  the population of dedifferentiated melanoma cells,  $T(t)$  the population of active T cells, and  $A(t)$  the population of cytokines  $TNF_\alpha$  at time  $t$ .

The growth phase of the disease ( $t < 70$ ) is characterized by the reproduction and death of melanoma cancer cells ( $M(t), D(t)$ ) plus the natural switch between these two cancer cell populations. At this stage, there are no active T cells nor cytokines  $TNF_\alpha$  ( $T(t) = 0, A(t) = 0$ ). The evolution of  $M(t)$  and  $D(t)$  is modeled by birth and death processes [19] including additional terms modeling the switches between the two cancer cell populations. The model described here corresponds to that of the control mice. It starts from  $(M(0) = M_0, D(0) = 0)$  with  $M_0$  the initial quantity of differentiated melanoma cells.

At time  $t = 70$  (beginning of treatment), a dose  $d_{70}$  of the T cell stimulant is injected in the system activating 2000 T cells ( $T(70) = 2000$ ). Then, all the four populations ( $M(t), D(t), T(t), A(t)$ ) evolve starting with initial conditions  $(M(70), D(70), T(70) = 2000,$

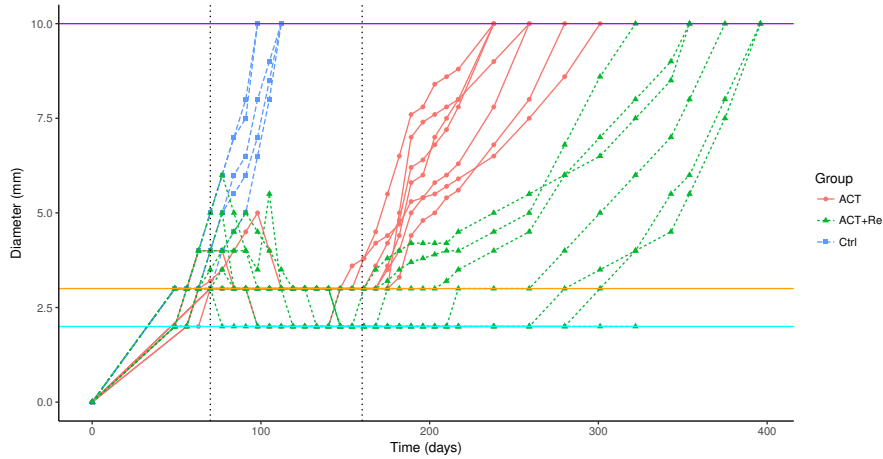


FIGURE 3. Tumor diameter (mm) along time (days) in the groups CTRL (dashed line in blue), ACT (solid line in red), ACT+Re (dotted line in green). The three types of censorship are indicated by the horizontal lines at diameter = 1.99 mm, 3 mm and 10 mm. The treatment at the 70th day and the re-treatment at the 160th day (for ACT+Re mice) are indicated by the vertical dotted lines.

$A(70) = 0$ ). The system models the evolution of differentiated melanoma cells  $M(t)$  (preys) in the presence of active T cells  $T(t)$  (predators) as a predator-prey framework. An additional natural exhaustion of active T cells is modeled by a simple death process. A deterministic production of cytokines  $A(t)$  occurs at each T cell reproduction event while the death of cytokines is modeled by a death process. An additional cytokine induced switch from a differentiated melanoma cell to a dedifferentiated one is also modeled. The model described at this stage corresponds to that of the group ACT.

At time  $t = 160$ , an additional dose  $d_{Re}$  of the T-cell stimulant is injected in the system for the mice in the group ACT+Re activating 2000 T cells ( $T(160) = T(160) + 2000$ ). The retreatment phase is modeled like the treatment phase by starting with initial conditions  $(M(160), D(160), T(160) = T(160) + 2000, A(160))$ .

Figure 4 describes the dynamics of the process during the treatment phase and shows the events occurring during this phase (see Section 2.2 of [4] for more details on the stochastic model and its construction).

All the events in the stochastic model (natural or therapy induced birth, death and switch) occur after exponential waiting times regulated by rate parameters. The parameters  $b_M$  and  $b_D$  in Figure 4 represent thus the birth rate of differentiated (respectively dedifferentiated) melanoma cells and correspond to the inverse of the average waiting time before observing the birth of a new differentiated (respectively dedifferentiated) melanoma cell. Similarly,  $d_M$  and  $d_D$  correspond to the natural death rate of differentiated (respectively dedifferentiated) melanoma cells while  $s_{MD}$  and  $s_{DM}$  represent respectively the switching rates from differentiated melanoma cells to dedifferentiated one and the inverse. The parameters  $b_T$  and  $d_T$  are respectively the birth and exhaustion rates of active T cells. To a certain extent,  $b_T$  can be seen as an effective parameter corresponding to  $b_T = b_T^0 - d_T^0$  with  $b_T^0$  and  $d_T^0$  respectively the therapy induced birth and exhaustion rates of active T

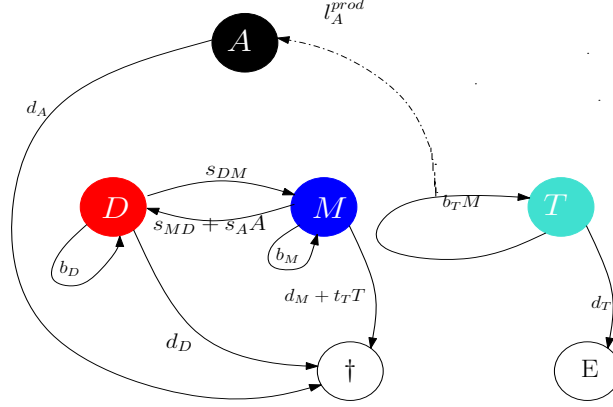


FIGURE 4. Dynamics of the stochastic process: natural and therapy induced birth/death of cells, T cell exhaustion, switches between the two types of melanoma cells and rate parameters associated to these events.  $M$  for differentiated melanoma cells;  $D$  for dedifferentiated melanoma cells;  $T$  for T cells;  $A$  for cytokines  $TNF_\alpha$ .  $\dagger$  symbolizes the death of cancer cells and cytokines;  $E$  symbolizes the exhaustion of T cells. The orientation of the arrow indicates the sense of the evolution of the population (an arrow with the initial and end points on the same population indicates a reproduction in this population). The values above the arrows represent the rate parameters which correspond to the inverse of the waiting times before the related-events occur [4].

cells. Indeed, the differentiated melanoma cells secrete a substance that exhausts active T cells with a rate  $d_T^0$  in addition to their natural exhaustion rate  $d_T$ . The therapy induced death of the differentiated melanoma cells is regulated by the rate parameter  $t_T$  while  $d_A$  corresponds to the natural death rate of the cytokines  $TNF_\alpha$ . The product  $l_A^{prod} \times b_T$  represents the therapy induced production rate of the cytokines and  $s_A$  is associated with the additional switching from differentiated melanoma cells to dedifferentiated one induced by the cytokines. We estimate these parameters as well as the initial quantity  $M_0$  of differentiated melanoma cells which value is not fixed from one mouse to another.

**3.2. Large population limit.** The dynamics of the stochastic model converges in the limit of large population of cells to the solution of the deterministic differential system [4]:

$$\begin{cases} \dot{\mathbf{n}}_M = (b_M - d_M)\mathbf{n}_M - s_{MD}\mathbf{n}_M + s_{DM}\mathbf{n}_D - s_A\mathbf{n}_A\mathbf{n}_M - t_T\mathbf{n}_T\mathbf{n}_M \\ \dot{\mathbf{n}}_D = (b_D - d_D)\mathbf{n}_D + s_{MD}\mathbf{n}_M - s_{DM}\mathbf{n}_D + s_A\mathbf{n}_A\mathbf{n}_M \\ \dot{\mathbf{n}}_T = -d_T\mathbf{n}_T + b_T\mathbf{n}_M\mathbf{n}_T \\ \dot{\mathbf{n}}_A = -d_A\mathbf{n}_A + l_A^{prod}b_T\mathbf{n}_M\mathbf{n}_T \end{cases} \quad (3.1)$$

with initial condition  $(n_{M_0}, n_{D_0}, n_{T_0}, n_{A_0})$ . The quantity  $\mathbf{n}_X(t) \in \mathbb{R}$  (with  $X = M, D, T$  or  $A$ ) represents the quantity of  $X$  at time  $t$  and  $\dot{\mathbf{n}}_X$  represents the variation of this quantity along time. Note that we work in this paper on a simplified version of the initial model [4] which contains some competition terms (in the framework of a logistic birth and death processes). We remove the competition terms from the model as they cannot be estimated from the data. Indeed, mice are killed before the tumor size (number of cancer cells) can reach the value of the (non trivial) fixed point regulated by the competition terms. To

avoid the problem of identifiability, new parameters are introduced:  $r_M = b_M - d_M$  and  $r_D = b_D - d_D$ . To ease the notations, we set  $d_M = d_D = 0$  ( $r_M = b_M$  and  $r_D = b_D$ ), keeping in mind that only the difference between birth and death rates of melanoma cells can be estimated from the data.

The different phases of the therapy are similar to the ones of the stochastic model. During the growth phase ( $t < 70$ ), only the populations of cancer cells  $n_{M(t)}$  and  $n_{D(t)}$  evolve ( $n_{T(t)} = 0$ ,  $n_{A(t)} = 0$ ). All the parameters associated with the treatment are then equal to zero. At time  $t = 70$ , the quantity of active T cells is set to  $n_{T(70)} = d_{70}$ . All the four populations of cells ( $n_{M(t)}$ ,  $n_{D(t)}$ ,  $n_{T(t)}$ ,  $n_{A(t)}$ ) evolve. At this stage, the model (3.1) corresponds to the dynamics of the ACT group. For the group ACT+Re, an additional quantity of active T cells is added in the system at  $t = 160$  ( $n_{T(160)} = n_{T(t)} + d_{Re}$ ).

## 4. STUDY OF THE RELAPSE

### 4.1. Parameter estimation.

4.1.1. *Mixed effects model.* The parameters are estimated by analyzing the data of all mice simultaneously. To take into account the inter-mice variability, a NonLinear Mixed Effects regression Model (NLMEM) is used [28]. Parameter estimation with NLMEMs is difficult since the likelihood function does not have an explicit form. When the regression function of the NLMEM is the stochastic model, the high dimension of the event space prevents to compute the likelihood. Thus, the parameter estimation is based on the maximization of the likelihood function of the deterministic model (3.1).

Let us define  $y_i = (y_{i1}, \dots, y_{in_i})$  where  $y_{ij}$  is the (noisy) measurement of the tumor diameter value for the mouse  $i$  at time  $t_{ij}$ ,  $i = 1, \dots, N$ ,  $j = 1, \dots, n_i$ , and set  $y = (y_1, \dots, y_N)$ . The NLMEM is defined by:

$$y_{ij} = f(\psi_i, t_{ij}) + \epsilon_{ij}, \quad \epsilon_i \sim \mathcal{N}(0, \sigma^2 I_{n_i}) \quad \text{and} \quad \psi_i = \mu + \eta_i, \quad \eta_i \sim \mathcal{N}(0, \Omega), \quad (4.1)$$

where  $\epsilon_i = (\epsilon_{i1}, \dots, \epsilon_{in_i})$  represents the residual error ;  $\mu = (n_{M_0}, r_M, r_D, \dots, s_{MD}, s_{DM})$  is a vector of fixed effects;  $\eta_i = (n_{M_0_i}, r_{M_i}, r_{D_i}, \dots, s_{MD_i}, s_{DM_i})$  is a vector of random effects independent of  $\epsilon_i$ ;  $\psi_i$  represents the vector of individual regression parameters ;  $f(\psi_i, t) = (n_M(\psi_i, t) + n_D(\psi_i, t))^{\frac{1}{3}}$  is a function describing the tumor diameter (up to some constant), with  $n_M$  and  $n_D$  being solution of the non-linear system (3.1);  $\sigma^2$  is the residual variance;  $I_{n_i}$  the identity matrix of size  $n_i$ ;  $\Omega$  the variance matrix of the random effects quantifying variability between the mice. We note  $\theta = (\mu, \Omega, \sigma^2)$  the parameters to be estimated. A biological constraint [22] states that the natural switch rate from a dedifferentiated melanoma cell to a differentiated melanoma cell ( $s_{DM}$ ) is greater than the inverse rate ( $s_{MD}$ ). This constraint is taken into account by estimating  $s_{DM_p}$  such that  $s_{DM} = s_{DM_p} + s_{MD}$  with  $s_{DM_p} > 0$ .

The SAEM-MCMC algorithm which combines the Stochastic Approximation Expectation Maximization algorithm [12] with an Markov chain Monte Carlo procedure adapted to censored data [21, 33], implemented under the software MONOLIX [24] allows to estimate the parameters of NLMEMs. We analyze the three groups of mice separately. The parameters to be estimated for the group CTRL are  $r_M$ ,  $r_D$ ,  $s_{MD}$ ,  $s_{DM}$ ,  $n_{M_0}$  and  $\sigma$ . For



| Parameters          | CTRL            | ACT            | ACT+Re          |
|---------------------|-----------------|----------------|-----------------|
| $r_M$               | 0.0819 (0.0699) | 0.0852 (0.131) | 0.0995 (0.125)  |
| $r_D$               | 0.0749 (0)      | 0.0523 (0)     | 0.0319 (0.154)  |
| $s_{MD}$            | 0.0082 (0)      | 0.0001 (0)     | 1.04e-05 (0)    |
| $s_{DM_p}$          | 0.0011 (0)      | 0.0011 (0)     | 0.0011 (0)      |
| $b_T$               |                 | 0.0006 (0)     | 0.0005 (0.404)  |
| $l_A^{\text{prod}}$ |                 | 0.5390 (0)     | 0.2520 (0)      |
| $t_T$               |                 | 0.0441 (0)     | 3.0200 (0)      |
| $d_T$               |                 | 0.0434 (0.318) | 0.0041 (1.71)   |
| $d_A$               |                 | 0.0288 (0.128) | 0.0307 (0.0569) |
| $s_A$               |                 | 65.600 (0.861) | 5.8600 (5.29)   |
| $n_{M_0}$           | 0.2150 (0.207)  | 0.0340 (1.1)   | 0.0361 (0.113)  |
| $\sigma$            | 0.4380          | 0.5000         | 0.4730          |

TABLE 1. Population parameters and inter-mice variances (in brackets) estimated for the groups CTRL, ACT, and ACT+Re.  $\sigma$  represents the residual error parameter. The values of  $\Omega$  (inter-subject variability) associated to parameters without random effect is equal to zero.

the group ACT and ACT+Re, the additional parameters related to the therapy are  $b_T$ ,  $l_A^{\text{prod}}$ ,  $t_T$ ,  $d_T$ ,  $d_A$ ,  $s_A$ . Initially, random effects are applied to all the parameters. According to the results of likelihood ratio tests on the significance of these effects, we remove the random effects on some of the parameters. The concerned parameters are  $r_D$ ,  $s_{MD}$ ,  $s_{DM}$  for the group CTRL;  $r_D$ ,  $s_{MD}$ ,  $s_{DM}$ ,  $b_T$ ,  $l_A^{\text{prod}}$ ,  $t_T$  for the group ACT and  $s_{MD}$ ,  $s_{DM}$ ,  $l_A^{\text{prod}}$ ,  $t_T$  for the group ACT+Re.

4.1.2. *Results.* Table 1 presents the estimates (population mean and inter-mice standard deviation) for the groups CTRL, ACT and ACT+Re. Figure 5 show the individual fit of the evolution of the tumor diameter along time for a mouse in the group ACT (other individual fits are provided in appendix). Data are well fitted and the growth and treatment phases are well captured. Some parameters have a large inter-mice standard deviation. This is mainly due to the small number of data compared to the number of parameters to be estimated. The estimations have been validated with graphical validation (fits, observations vs predictions, SAEM convergence graphics in appendix) and the calculation of standard errors associated with the parameters through an estimation of the Fisher Information Matrix (FIM).

4.1.3. *Discussion.* From one group to another, the values of some parameters remain roughly the same (e.g.  $r_M$ ,  $r_D$ ,  $l_A^{\text{prod}}$ ,  $d_A$ ,  $b_T$ ,  $\sigma$ ) and for others, differences are noted ( $t_T$ ,  $s_A$ ,  $d_T$ ). From a biological point of view, the switching rate from differentiated melanoma cells to dedifferentiated ones should be higher than the killing rate of differentiated cells by T cells. We note that this remark is supported by the estimated parameters ( $s_A > t_T$ ).

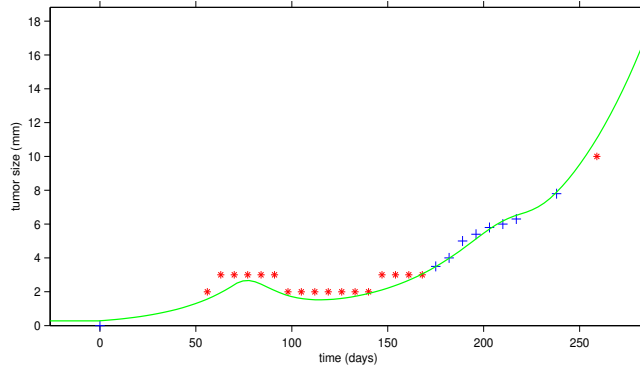


FIGURE 5. Individual fit for a mouse of the group ACT. The blue points represent the no censored observations, the red points the censored observations, the green line the fitted tumor size dynamic.

## 4.2. T cell exhaustion.

4.2.1. *Simulation.* The T cell exhaustion is defined by the event  $\{T_t \leq S = 0, t \leq t_F\}$  where  $T_t$  is the active T cell population at time  $t$ ,  $S = 0$  the exhaustion threshold,  $t \leq t_F$  a condition to have the exhaustion in a finite time. T cell exhaustion can only happen in the stochastic system and not in its deterministic limit. This follows from the analyticity of the solutions to (3.1), given that  $T_t(0) > 0$ .

The code used to simulate the stochastic dynamics is based on the Gillespie algorithm described in [4]. The simulation over reasonable intervals of time generates millions of stochastic events (natural or therapy induced birth, death, switches) which necessitates a large computing time. The code has been written in C++ and ran under the software R [30] through the package Rcpp [14].

4.2.2. *Estimation of T cell exhaustion probability.* We want to estimate the exhaustion probability  $p = \mathbb{P}(T_t \leq S = 0, t \leq t_F)$ . Let  $u = \mathbb{1}_{T_t \leq S = 0}$ . Using a Monte Carlo method, an estimation of the T cell exhaustion probability is given by  $\hat{p} = \frac{\sum_{k=1}^{N_T} u_k}{N_T}$  with  $N_T$  the total number of simulations. The main drawback with this Monte Carlo method is the fact that a large number  $N_T$  of simulations is needed when the probability  $p$  is very small. The method is then not suitable for rare event probability estimation because the variance on the estimation diverges when the probability tends to zero [25]. To reduce the variance for very small probabilities estimation, an alternative is the Importance Splitting (IS) algorithm designed for rare event probability estimation [10, 18, 25]. IS gradually calculates the probability of reaching the threshold  $S$  (the rare event) through the calculation of the probability of reaching intermediate thresholds easier to reach than  $S$ . For the event  $\{T_t \leq S = 0, \text{ for } t \leq t_F\}$ , the probability  $\mathbb{P}(T_t \leq S = 0, t \leq t_F)$  is calculated according to the splitting principle by

$$\mathbb{P}(T_t \leq S = 0, t \leq t_F) = \prod_{k=1}^m p_k \quad (4.2)$$

with  $p_1 = \mathbb{P}(T_t \leq S_1, t \leq t_F)$  and  $p_k = \mathbb{P}(T_t \leq S_k \mid T_s \leq S_{k-1}, s \leq t \leq t_F)$  for  $k = 2, \dots, m$ . The  $S_k$  ( $k < m$ ) are the intermediate thresholds and  $S_m = S$  the exhaustion threshold. The IS algorithm consists at each iteration  $k$ : in the simulation of  $N_T$  trajectories of the process  $T_t$  and the estimation (by Monte Carlo) of the intermediate probability  $p_k$  by considering the number  $N_{S_k}$  of trajectories which reach an intermediate threshold  $S_k$  before the time  $t_F$ :  $p_k = \frac{N_{S_k}}{N_T}$ . To pass from iteration  $k$  to iteration  $k + 1$ ,  $N_T$  trajectories are sampled from the  $N_{S_k}$  trajectories having reached the threshold  $S_k$  (by allowing replacement in the sampling) and run the  $N_T$  new trajectories in order to reach the next threshold  $S_{k+1}$ . In our setting, we consider that there is T cell exhaustion at time  $t$  when the quantity of T cells at  $t$  reaches  $S_5 = 0$ . We define four other intermediate thresholds  $S_1 = 7 \times 10^{-5}$  (or 0.35% of the initial quantity of active T cells),  $S_2 = 5 \times 10^{-5}$  (0.25% of  $T(70)$ ),  $S_3 = 3 \times 10^{-5}$  (0.15% of  $T(70)$ ), and  $S_4 = 2 \times 10^{-5}$  (0.1% of  $T(70)$ ). For all the T cell exhaustion probability calculation, we set  $N_T$  to 1000.

**4.2.3. Results.** The T cell exhaustion probability estimated by the IS algorithm is zero (very close to absolute zero) when considering the population parameters of the ACT or the ACT+Re mice (as well as for the individual parameters of each mouse in the two groups). We can then consider that the relapses observed in the experimental data are not due to T cell exhaustion but only to the switch from differentiated to the dedifferentiated cells. This consideration is nevertheless to be taken with caution due to the large inter-subject variances on the estimated parameters. Indeed, among the parameters with non-zero variance presented in Table 1, the parameter  $d_T$  (death rate of T cells) changes significantly the value of the T cell exhaustion probability. We thus estimate the exhaustion probability as a function of  $d_T$  in its estimation range ( $\hat{\mu}_{d_T^{ACT}} \pm \hat{\Omega}_{d_T^{ACT}} = ]0, 0.36]$ ) when the other parameters are fixed to their estimated population values, see Figure 6. We observe that the T cell exhaustion probability increases with  $d_T$ , and even reaches large values. This corroborates the hypothesis in [4] which asserts that there exist biological parameters (here, parameters estimated from biological data) for which the probability of disease relapse due to T cell exhaustion is high. Moreover, Figure 6 allows to visualize the link between the probability of T cell exhaustion and the value of the minimum of the deterministic T cell dynamics (which decreases when  $d_T$  increases).

## 5. TREATMENT OPTIMIZATION

**5.1. Criteria to optimize the treatment.** The kind of relapse we can act on without changing the medical setup is the relapse due to T cell exhaustion. We thus want to minimize the probability of T cell exhaustion, i.e. to keep the minimum of the T cell trajectory as high as possible in order to avoid that the stochastic fluctuations cross the exhaustion threshold  $S = 0$ . The treatment parameters to be optimized are the treatment dose  $d_{70}$ , the retreatment time  $t_{Re}$  and dose  $d_{Re}$ . The optimization is done with the deterministic model by exploiting the link between the exhaustion probability and the depth of the T cell deterministic minimum, see Figure 6. The cost function (to be maximized) is defined by the function  $g$  which returns the minimum of the T cell trajectory:  $g(t) = \min n_{T_t}$  with  $n_{T_t}$  solution of the system (3.1). We consider two optimization procedures: the first one

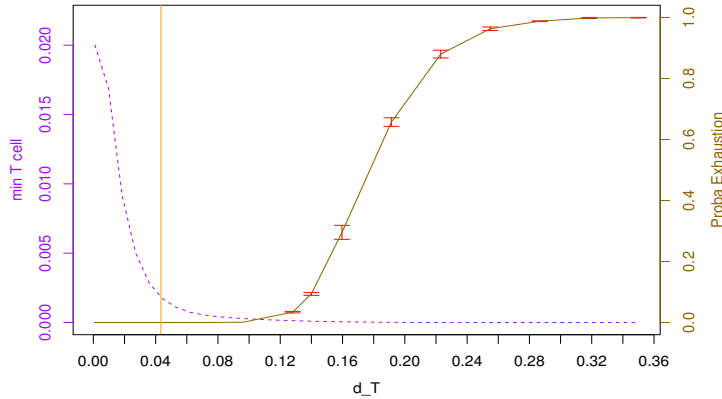


FIGURE 6. Evolution of T cell exhaustion probability (solid line) and the deterministic global minimum of T cells (dashed line) according to the death rate of T cells ( $d_T$ ) in the group ACT. For each value of  $d_T$ , the T cell exhaustion probability is computed 5 times and the mean is represented with an error bar (corresponding to mean  $\pm$  standard deviation). The vertical line at  $d_T = 0.0434$  indicates the population value of  $d_T$ .

is performed on the group ACT and leads in the optimal treatment dose  $d_{70}^{\text{opt}ACT}$  (and the associated time  $t_R$  corresponding to the time when  $g(t)$  reaches its maximum). Here the function  $g$  depends on the dose  $d_{70}$  injected at time  $t = 70$ . We thus denote the function  $g(t, d_{70}) = \min n_{T_i}(d_{70})$ . The treatment is optimized by the following criteria:

$$d_{70}^{\text{opt}ACT} = \arg \max_{d_{70} \in [d_{\min}, d_{\max}]} g(t, d_{70}), \quad t \leq t_F^{ACT} = 300, \quad (5.1)$$

we restrict the dose optimization interval to  $[d_{\min}, d_{\max}]$ . The second optimization procedure is performed on the group ACT+Re and provides the optimal retreatment dose  $d_{Re}^{\text{opt}ACT+Re}$  using the dose  $d_{70}^{\text{opt}ACT}$  as the treatment dose ( $d_{70}^{\text{opt}ACT+Re} = d_{70}^{\text{opt}ACT}$ ) and its associated time  $t_R$  as optimal retreatment time ( $t_{Re}^{\text{opt}} = t_R$ ).

$$d_{Re}^{\text{opt}} = \arg \max_{d_{Re} \in [d_{\min}, d_{\max}]} g(t, d_{70}^{\text{opt}ACT+Re}, d_{Re}, t_{Re}^{\text{opt}}), \quad t_{Re}^{\text{opt}} \leq t \leq t_F^{ACT+Re} = 400 \quad (5.2)$$

**Remark:** As shown in Figure 7, the treatment dose as well as the value of the initial quantity of differentiated melanoma cells  $M_0$  change significantly the T cell global minimum, and therefore, the T cell exhaustion probability. Moreover,  $M_0$  can be seen as an indicator of different initial stages of the disease. Thus, it is a relevant variable to present our results.

**5.2. Optimal values computation.** The optimization can be done by using the package "optim" allowing to perform box-constrained optimization [8] under the software R [30], and graphics plotting the evolution of T cell minimum along time for different values of  $M_0$ , see Figures 7, 8, 9. The optimization is performed with the deterministic model using the population estimated parameters in Table 1 and the initial values:  $t_0 = 0$  representing

the initial time;  $M_0 \in \{0.007, 0.020, 0.034, 0.046\}$  different initial values of differentiated melanoma cells;  $D_0 = 0$  the initial quantity of dedifferentiated melanoma cells;  $A_0 = 0$  the initial quantity of  $TNF_\alpha$ ;  $d_{70}^{\text{initial}} = d_{Re}^{\text{initial}} = 0.02$  the initial treatment doses (optimized over the interval  $[d_{\min}, d_{\max}] = [0.005, 0.04]$ ) and  $t_{Re}^{\text{initial}} = 160$  the initial restimulation time.

**5.3. Results.** The optimal values are given in Table 2. The column ACT corresponds to the optimization criteria (5.1) and the column ACT+Re, to (5.2). The optimal treatment parameters are indicated in Figures 7, 8, 9. Even if the T cell exhaustion probability is

| $M_0$ | Parameters            | ACT     | ACT+Re  |
|-------|-----------------------|---------|---------|
| 0.007 | $d_{70}^{\text{opt}}$ | 0.01123 | 0.01123 |
|       | $d_{Re}^{\text{opt}}$ | -       | 0.04000 |
|       | $t_{Re}^{\text{opt}}$ | -       | 175.42  |
| 0.020 | $d_{70}^{\text{opt}}$ | 0.00549 | 0.00549 |
|       | $d_{Re}^{\text{opt}}$ | -       | 0.04000 |
|       | $t_{Re}^{\text{opt}}$ | -       | 165.33  |
| 0.034 | $d_{70}^{\text{opt}}$ | 0.00500 | 0.00500 |
|       | $d_{Re}^{\text{opt}}$ | -       | 0.04000 |
|       | $t_{Re}^{\text{opt}}$ | -       | 157.51  |
| 0.046 | $d_{70}^{\text{opt}}$ | 0.04000 | 0.04000 |
|       | $d_{Re}^{\text{opt}}$ | -       | 0.04000 |
|       | $t_{Re}^{\text{opt}}$ | -       | 158.47  |

TABLE 2. Summary table of optimization results for four given values of the initial quantity of differentiated melanoma cells  $M_0$  in the groups ACT and ACT+Re.

very close to zero with the estimated population parameters, optimizing the treatment to keep the deterministic minimum as high as possible is still beneficial since it allows to further delay the T cell exhaustion time, therefore to further delay the possible relapse due to this exhaustion. From an experimental point of view, the initial dose  $d^{\text{initial}} = 0.02$  is "well chosen" for good tumor control. This leads us to set  $d_{\min}$  and  $d_{\max}$  not too far from the dose  $d^{\text{initial}}$ . For the first three considered values of  $M_0$ , the optimal dose  $d_{70}^{\text{opt}}$  is smaller than the initial value  $d_{70}^{\text{initial}}$  and for the fourth value of  $M_0$  (the biggest one), the optimal treatment dose corresponds to  $d_{\max}$ . These different optimal values are induced by the predator-prey cycles between T cells and differentiated melanoma cells. We note that even if the second and third optimal doses  $d_{70}^{\text{opt}}$  are very low (close to  $d_{\min}$ ), they however lead to reasonable restimulation times  $t_{Re}^{\text{opt}}$ . Regarding the optimal restimulation dose  $d_{Re}^{\text{opt}}$ , it is equal to  $d_{\max}$  for each of the four  $M_0$  values and it contributes to further reduce the depth of the deterministic minimum, i.e., to further reduce the probability of T-cell exhaustion for ACT+Re mice.

It has been biologically observed that when the tumor size exceeds a certain threshold at the beginning of the treatment ( $t = 70$ ), the tumor control is less efficient even if we add more T cells. To check this with our model, we represent in Figure 10 the tumor size

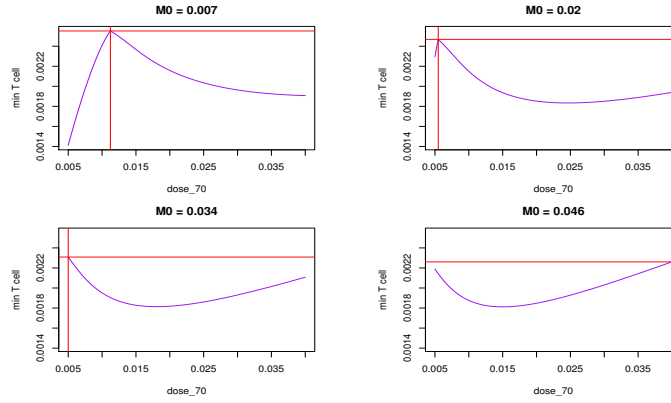


FIGURE 7. Evolution of the T cell global minimum according to the treatment dose  $d_{70}$  in the group ACT for different values of  $M_0$ . The vertical red line indicates the dose  $d_{70}^{\text{opt}^{\text{ACT}}}$  which maximizes the function  $g(t, d_{70})$ .

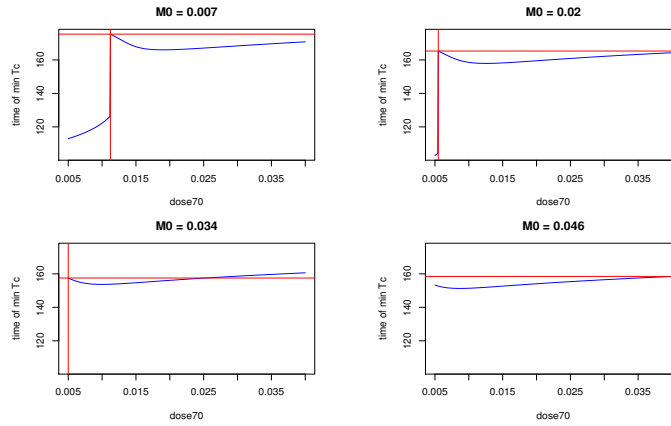


FIGURE 8. Evolution of the time associated to the T cell global minimum according to the treatment dose  $d_{70}$  in the group ACT for different values of  $M_0$ . The vertical red line indicates the dose  $d_{70}^{\text{opt}^{\text{ACT}}}$  which maximizes the function  $g(t, d_{70})$  and the horizontal red line indicates the time  $t_R$  associated to this dose.

dynamics in the group ACT for different values of  $M_0$  when the treatment dose  $d_{70}$  is fixed at its maximum value  $d_{70} = 0.04$  (one of the calculated optimal doses). For  $d_{70}^{\text{opt}} = 0.04$  (as well as for the other three optimal doses), the tumor size reaches the critical threshold of 10 mm meaning that a relapse is observed for each of these doses during the ACT therapy. However, these relapses are not due to T cell exhaustion, see Figures 6 and 7 which show the T cell exhaustion probability for different depths of the deterministic minimum. They are therefore attributed to the growth of dedifferentiated cells which are not killed by T cells. Nevertheless, let us focus on the effects of the tumor control achieved through the minimization of T cell exhaustion probability. Note that the larger the  $M_0$ , the faster the tumor growth. Note also that the use of large treatment doses  $d_{70}$  does not impact considerably the evolution of the tumor size regardless of this size value at  $t = 70$ . The tumor growth is just slightly slower for high doses  $d_{70}$ .

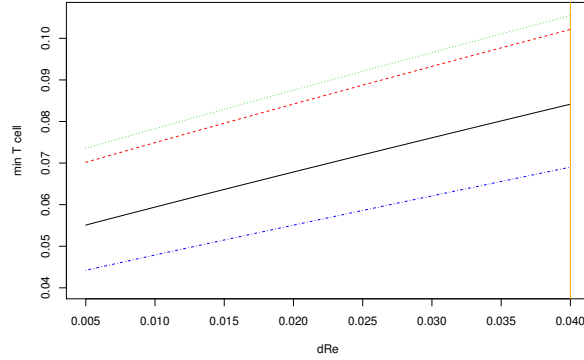


FIGURE 9. Evolution of the T cell global minimum according to the retreatment dose  $d_{Re}$  in the group ACT+Re for different values of  $M_0$  and for  $t \geq t_{Re}^{opt}$  (retreatment phase).  $M_0 = 0.007$  in solid line (black),  $M_0 = 0.02$  in dashed line (red),  $M_0 = 0.034$  in dotted line (green),  $M_0 = 0.046$  in dotdashed line (blue). The vertical orange line indicates the dose  $d_{Re}^{opt_{ACT+Re}}$  which maximizes the function  $g(t, d_{70})$ .

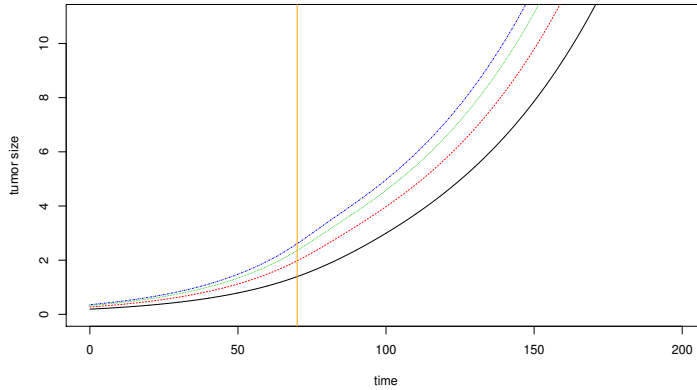


FIGURE 10. Tumor size along time for different values of  $M_0$  in the group ACT, dose  $d_{70} = 0.04$ .  $M_0 = 0.007$  in solid line (black),  $M_0 = 0.02$  in dashed line (red),  $M_0 = 0.034$  in dotted line (green),  $M_0 = 0.046$  in dotdashed line (blue). The vertical line (orange) at  $t = 70$  indicates the beginning of treatment.

We represent in Figure 11 the T cell and differentiated melanoma cell population dynamics for different doses to show the treatment effect on the disease for  $M_0 = 0.02$  (almost the same Figure for  $M_0 = 0.034, 0.046$ ). We note that depending on the dose value, differentiated cells are differently impacted by T cells (treatment) in predator-prey cycles. Thus, the greater the dose, the more the growth of the differentiated cells is slowed down at the beginning of the treatment. We also note that for each of the four doses in Figure 11, the deterministic T cell curve grows up at the end. In the stochastic model, when the

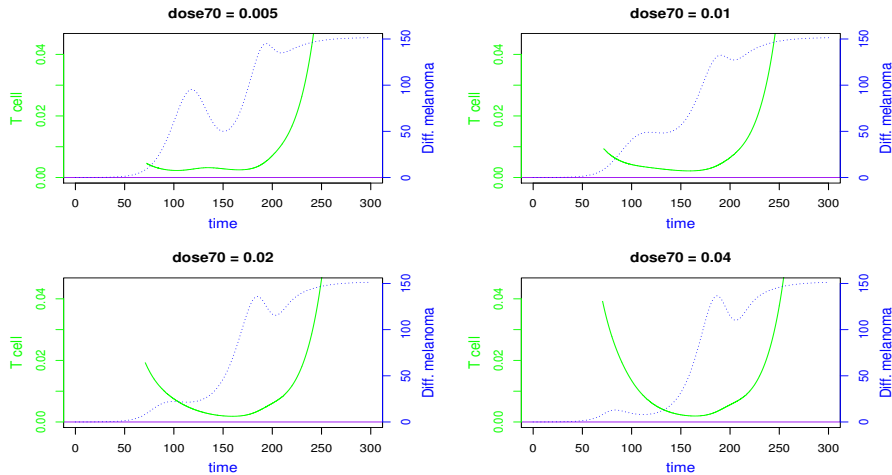


FIGURE 11. T cell (solid line in green) and differentiated melanoma cell (dotted line in blue) along time for different doses in the group ACT,  $M_0 = 0.02$ .

minimum of T cells is sufficiently low, stochastic fluctuations may in some cases cross the exhaustion threshold  $S = 0$ .

Moreover, Figure 11 highlights an interesting phenomenon: due to predator-prey cycles, the T cell dynamics exhibits several local minima along time (see for  $d_{70} = 0.005$  in Figure 11). This is well highlighted in Figure 12 by zooming in on the T cell local minima for small doses  $d_{70}$  with  $M_0 = 0.007$ . For T cell curves with several local minima, the first minimum is generally the deepest (the global minimum). However, there may be some cases where enlarging the initial dose of T cells shifts up the height at the first minimum, thus making the second minimum the global one. In these cases, the position of the global minimum as a function of the initial dose exhibits a discontinuity, as it can be seen on Figures 7, 8,  $M_0 = 0.007, 0.02$ . This affects the treatment optimization in a non-trivial way.

## 6. DISCUSSION

In cancer treatment, resistance to therapy is a major problem. Understanding the mechanism of this resistance is then crucial. The estimation of parameters of the stochastic model developed in [4] using biological data was essential in order to provide an accurate model, since the parameters have been only calibrated numerically in [4]. This estimation allows us to simulate realistic stochastic phenomena arising in the therapy, mainly the relapse due to T cell exhaustion. Estimating the probability of this relapse was important since it allows to evaluate the quality of the treatment. Moreover, obtaining a non-negligible probability of exhaustion in a large portion of the biologically relevant parameter space indicates the pertinence of stochastic models compared to deterministic ones.

The treatment optimization part of our work is performed on the deterministic system, due to the too high programming cost in the stochastic setting. Of course, this prevents from taking into account the stochastic aspect of the problem. An alternative would be the



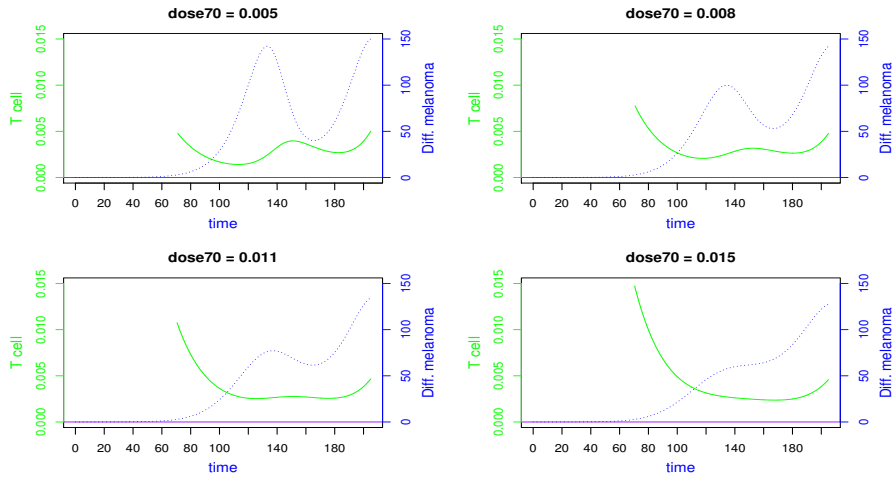


FIGURE 12. T cell (solid line in green) and differentiated melanoma cell (dotted line in blue) along time for different doses in the group ACT,  $M_0 = 0.007$ .

use of a diffusion approximation obtained from the deterministic model (addition of Brownian noise), which would allow to include a stochastic side in the problem while remaining very reasonable in the computational costs. This could also lead to other perspectives such as the estimation of the dynamics by a (stochastic) diffusion approximation of the initial stochastic model. The parameters estimated in the deterministic approximation could be still used as a priori knowledge in the context of a Bayesian estimation for example.

One of the main drawback of our study is that we propose an optimization of the treatment protocol which minimizes the probability of T cell exhaustion, while the presence of dedifferentiated melanoma (produced by the treatment) always leads to a relapse (even if T cells are not exhausted). To go beyond this problem, there are many prospects for improving treatment protocols. A first example is to introduce other types of T cells that could kill dedifferentiated melanoma (see [4] for a theoretical study) ; a second one consists in finding a way to act on the switch rate from differentiated to dedifferentiated melanoma. Indeed, if the switch rate from differentiated cells to dedifferentiated cells is well controlled in the therapy (and that the number of dedifferentiated cells is finally zero or much too low to cause a relapse), it will be enough to take in the current model ( $s_A = 0$ ) and the problem of complete healing of mice will come down to the control of T-cell exhaustion (as done in this paper). Thus, our work may have useful consequences on futur tumor treatment protocols.

## APPENDIX

**Figures of the group CTRL.**

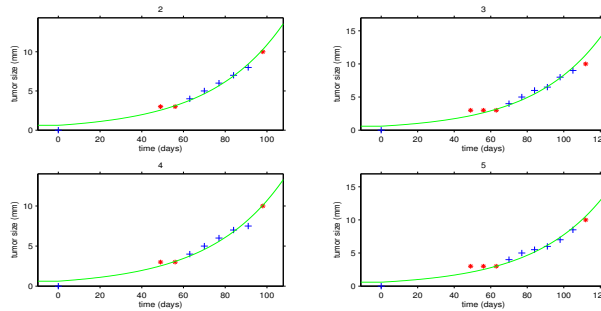


FIGURE 13. Individual fits for mice of the group CTRL. The blue points represent the no censored observations, the red points the censored observations, the green line the fitted tumor size dynamic.

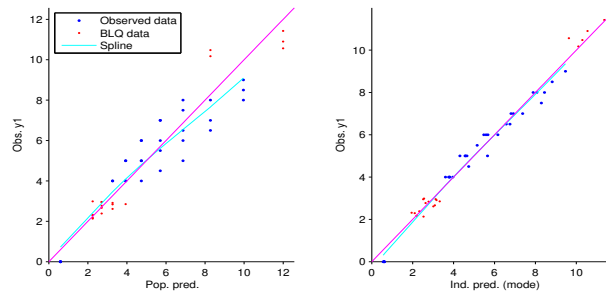


FIGURE 14. Individual predicted values versus observed values to assess the accuracy of the model for mice in the group CTRL. The blue points represents no censored observations, the red points the censored observations.

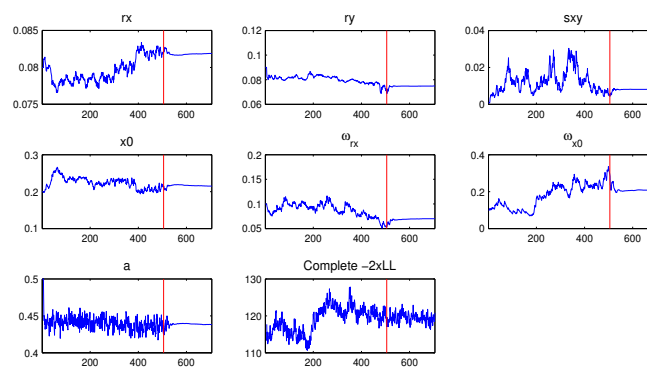


FIGURE 15. Convergence of the SAEM-MCMC algorithm during the estimation of the rate parameters in the group CTRL.

**Figures of the group ACT.**

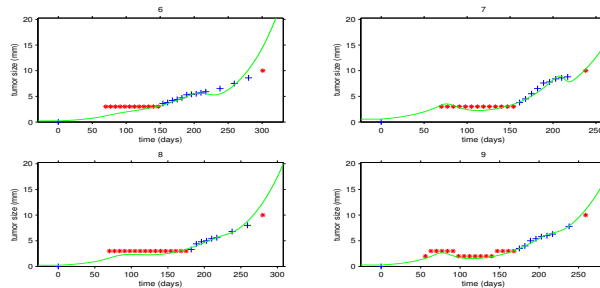


FIGURE 16. Individual fits for mice of the group ACT. The blue points represent the no censored observations, the red points the censored observations, the green line the fitted tumor size dynamic.

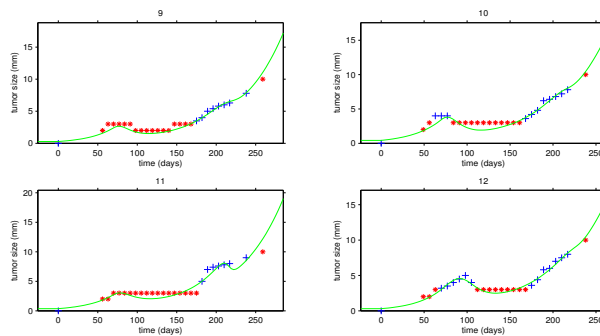


FIGURE 17. Individual fits for mice of the group ACT. The blue points represent the no censored observations, the red points the censored observations, the green line the fitted tumor size dynamic.

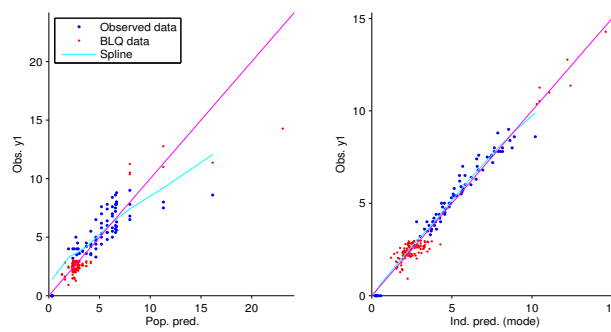


FIGURE 18. Individual predicted values versus observed values to assess the accuracy of the model for mice in the group ACT. The blue points represents no censored observations, the red points the censored observations.

**Figures of the group ACT+Re.**

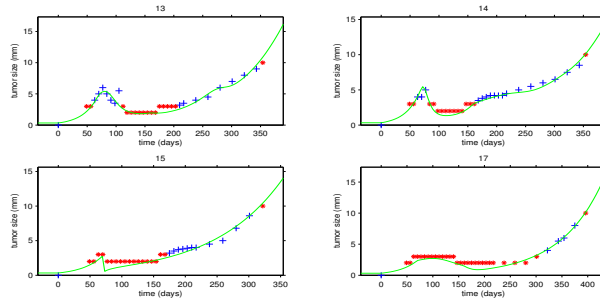


FIGURE 19. Individual fits for mice of the group ACT+Re. The blue points represent the no censored observations, the red points the censored observations, the green line the fitted tumor size dynamic.

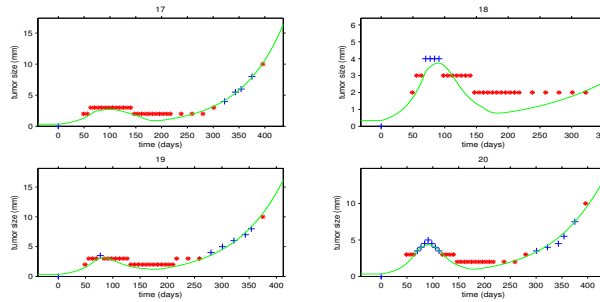


FIGURE 20. Individual fits for mice of the group ACT+Re. The blue points represent the no censored observations, the red points the censored observations, the green line the fitted tumor size dynamic.

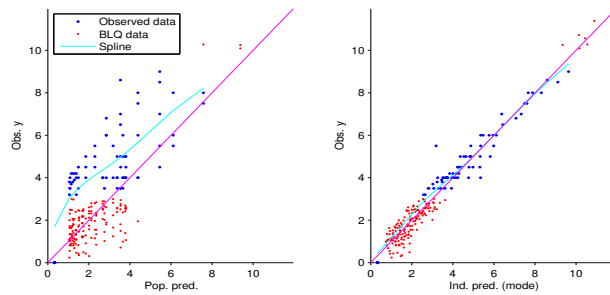


FIGURE 21. Individual predicted values versus observed values to assess the accuracy of the model for mice in the group ACT+Re. Blue points represents no censored observations, red points the censored observations.

## REFERENCES

- [1] R. Airley. *Cancer chemotherapy: basic science to the clinic*. John Wiley & Sons, 2009.
- [2] A. R. Anderson and M. Chaplain. Continuous and discrete mathematical models of tumor-induced angiogenesis. *Bulletin of mathematical biology*, 60(5):857–899, 1998.
- [3] E. N. Atkinson, R. Bartoszyński, B. W. Brown, and J. R. Thompson. On estimating the growth function of tumors. *Mathematical biosciences*, 67(2):145–166, 1983.
- [4] M. Baar, L. Coquille, H. Mayer, M. Hölzel, M. Rogava, T. Tüting, and A. Bovier. A stochastic individual-based model for immunotherapy of cancer. *Scientific Reports*, 2015.
- [5] D. Barbolosi, A. Benabdallah, F. Hubert, and F. Verga. Mathematical and numerical analysis for a model of growing metastatic tumors. *Mathematical biosciences*, 218(1):1–14, 2009.
- [6] A. A. Berryman. The origins and evolution of predator-prey theory. *Ecology*, 73(5):1530–1535, 1992.
- [7] L. J. Brant, S. L. Sheng, C. H. Morrell, G. N. Verbeke, E. Lesaffre, and H. B. Carter. Screening for prostate cancer by using random-effects models. *Journal of the Royal Statistical Society: Series A (Statistics in Society)*, 166(1):51–62, 2003.
- [8] R. H. Byrd, P. Lu, J. Nocedal, and C. Zhu. A limited memory algorithm for bound constrained optimization. *SIAM Journal on Scientific Computing*, 16(5):1190–1208, 1995.
- [9] P. Cattiaux, C. Christophe, S. Gadat, et al. A stochastic model for cytotoxic t. lymphocyte interaction with tumor nodules. *Journal of Mathematical Biology, in Revision*, 2(5), 2016.
- [10] F. Cérou and A. Guyader. Adaptive multilevel splitting for rare event analysis. *Stochastic Analysis and Applications*, 25(2):417–443, 2007.
- [11] M. Costa, C. Hauzy, N. Loeuille, and S. Méléard. Stochastic eco-evolutionary model of a prey-predator community. *Journal of mathematical biology*, 72(3):573–622, 2016.
- [12] B. Delyon, M. Lavielle, and E. Moulines. Convergence of a stochastic approximation version of the EM algorithm. *Annals of statistics*, pages 94–128, 1999.
- [13] S. Desmée, F. Mentré, C. Veyrat-Follet, and J. Guedj. Nonlinear mixed-effect models for prostate-specific antigen kinetics and link with survival in the context of metastatic prostate cancer: a comparison by simulation of two-stage and joint approaches. *The AAPS journal*, 17(3):691–699, 2015.
- [14] D. Eddelbuettel, R. François, J. Allaire, K. Ushey, Q. Kou, N. Russel, J. Chambers, and D. Bates. Rcpp: Seamless r and c++ integration. *Journal of Statistical Software*, 40(8):1–18, 2011.
- [15] J. Ferlay, I. Soerjomataram, R. Dikshit, S. Eser, C. Mathers, M. Rebelo, D. M. Parkin, D. Forman, and F. Bray. Cancer incidence and mortality worldwide: sources, methods and major patterns in globocan 2012. *International journal of cancer*, 136(5), 2015.
- [16] L. Hawley. Principles of radiotherapy. *British Journal of Hospital Medicine*, 74(Sup11):C166–C169, 2013.
- [17] K. R. Honerlaw, M. E. Rumble, S. L. Rose, C. L. Coe, and E. S. Costanzo. Biopsychosocial predictors of pain among women recovering from surgery for endometrial

- cancer. *Gynecologic oncology*, 140(2):301–306, 2016.
- [18] D. Jacquemart-Tomi, J. Morio, and F. L. Gland. A combined importance splitting and sampling algorithm for rare event estimation. *Proceedings of the 2013 Winter Simulation Conference, Washington 2013, Dec 2013, WASHINGTON, United States.*, 2013.
- [19] D. G. Kendall. On the generalized” birth-and-death” process. *The annals of mathematical statistics*, pages 1–15, 1948.
- [20] J. P. Klein and R. Bartoszynski. Estimation of growth and metastatic rates of primary breast cancer. *Mathematical Population Dynamics*, pages 397–412, 1991.
- [21] E. Kuhn and M. Lavielle. Coupling a stochastic approximation version of EM with an MCMC procedure. *ESAIM: Probability and Statistics*, 8:115–131, 2004.
- [22] J. Landsberg, J. Kohlmeyer, M. Renn, T. Bald, M. Rogava, M. Cron, M. Fatho, V. Lennerz, T. Wölfel, M. Hölzel, et al. Melanomas resist T-cell therapy through inflammation-induced reversible dedifferentiation. *Nature*, 490(7420):412–416, 2012.
- [23] B. D. Liebelt, G. Finocchiaro, and A. Heimberger. Principles of immunotherapy. *Handbook of clinical neurology*, 134:163–181, 2016.
- [24] Monolix. Monolix Users Guide Version 4.3.3, A software for the analysis of nonlinear mixed effects models, 2014.
- [25] J. Morio, R. Pastel, and F. L. Gland. An overview of importance splitting for rare event simulation. *European Journal of Physics*, 2010.
- [26] A. S. Novozhilov, F. S. Berezovskaya, E. V. Koonin, and G. P. Karev. Mathematical modeling of tumor therapy with oncolytic viruses: regimes with complete tumor elimination within the framework of deterministic models. *Biology direct*, 1(1):6, 2006.
- [27] A. Ochab-Marcinek. Pattern formation in a stochastic model of cancer growth. *arXiv:q-bio/0501007v2 [q-bio.CB]*, 2005.
- [28] J. Pinheiro and D. Bates. *Mixed-effects models in S and S-PLUS (statistics and computing)*. Springer, New York, 2000.
- [29] V. Quaranta, A. M. Weaver, P. T. Cummings, and A. R. Anderson. Mathematical modeling of cancer: the future of prognosis and treatment. *Clinica Chimica Acta*, 357(2):173–179, 2005.
- [30] R Core Team. *R: A Language and Environment for Statistical Computing*. R Foundation for Statistical Computing, Vienna, Austria, 2014.
- [31] M. S. Sabel, K. M. Diehl, and A. E. Chang. Principles of surgical therapy in oncology. *Oncology*, pages 58–72, 2006.
- [32] I. Sagiv-Barfi, D. K. Czerwinski, S. Levy, I. S. Alam, A. T. Mayer, S. S. Gambhir, and R. Levy. Eradication of spontaneous malignancy by local immunotherapy. *Science translational medicine*, 10(426):eaan4488, 2018.
- [33] A. Samson, M. Lavielle, and F. Mentré. Extension of the SAEM algorithm to left-censored data in nonlinear mixed-effects model: Application to HIV dynamics model. *Computational Statistics and Data Analysis*, 51(3):1562–1574, 2006.
- [34] A. Sottoriva and S. Tavaré. Integrating approximate bayesian computation with complex agent-based models for cancer research. In *Proceedings of COMPSTAT*, pages 57–66. Springer, 2010.

- [35] S. Sun, M. F. Wheeler, M. Obeyesekere, and C. W. Patrick. A deterministic model of growth factor-induced angiogenesis. *Bulletin of mathematical biology*, 67(2):313, 2005.
- [36] Y. Watanabe, E. L. Dahlman, K. Z. Leder, and S. K. Hui. A mathematical model of tumor growth and its response to single irradiation. *Theoretical Biology and Medical Modelling*, 13(1):6, 2016.
- [37] L. Willis, T. Alarcón, G. Elia, J. L. Jones, N. A. Wright, I. P. Tomlinson, T. A. Graham, and K. M. Page. Breast cancer dormancy can be maintained by small numbers of micrometastases. *Cancer research*, 70(11):4310–4317, 2010.

MODIBO DIABATE, LABORATOIRE JEAN KUNTZMANN, UNIV. GRENOBLE ALPES F-38000 GRENOBLE, FRANCE

*E-mail address:* modibo.diabate@univ-grenoble-alpes.fr

LOREN COQUILLE, UNIV. GRENOBLE ALPES, CNRS, INSTITUT FOURIER, F-38000 GRENOBLE, FRANCE

*E-mail address:* loren.coquille@univ-grenoble-alpes.fr

ADELIN SAMSON, LABORATOIRE JEAN KUNTZMANN, UNIV. GRENOBLE ALPES F-38000 GRENOBLE, FRANCE

*E-mail address:* adeline.leclercq-samson@univ-grenoble-alpes.fr